AD-A073 852 RICE UNIV HOUSTON TEX DEPT OF SPACE PHYSICS AND ASTRONOMY F/G 4/1
BIRKELAND CURRENTS AND RING CURRENTS IN THE COMPUTER SIMULATION--ETC(U)
FEB 79 M HAREL, R A WOLF, P H REIFF, M SMIDDY F19628-77-C-0005
UNCLASSIFIED SCIENTIFIC-1 AFGL-TR-79-0041 NL

| OF |
AD A073852

END
DATE FILMED
10-79
DDC

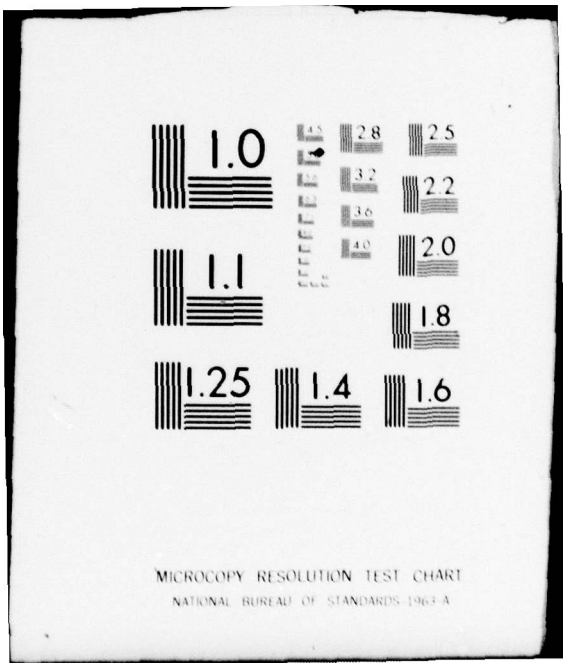
1.0
1.1
1.25
1.4
1.6
2.8
3.2
3.6
4.0
2.5
2.2
2.0
1.8
MICROCOPY RESOLUTION TEST CHART
NATIONAL BUREAU OF STANDARDS-1963-A

LEVEL II

13

AFGL-TR-79-0041

BIRKELAND CURRENTS AND RING CURRENTS IN THE COMPUTER SIMULATION OF THE SUBSTORM OF 19 SEPTEMBER 1976

M. Harel,
R.A. Wolf
P.H. Reiff
M. Smiddy

Department of Space Physics and Astronomy
Rice University
Houston, Texas 77001

7 February 1979

Scientific Report No. 1

AIR FORCE GEOPHYSICS LABORATORY
AIR FORCE SYSTEMS COMMAND
UNITED STATES AIR FORCE
HANSCOM AFB, MASSACHUSETTS 01731

Unclassified

SECURITY CLASSIFICATION OF THIS PAGE (When Data Entered)

REPORT DOCUMENTATION PAGE

READ INSTRUCTIONS BEFORE COMPLETING FORM

1. REPORT NUMBER: AFGL-TR-79-0041

2. GOVT ACCESSION NO.

3. RECIPIENT'S CATALOG NUMBER

4. TITLE (and Subtitle): Birkeland Currents and Ring Currents in the Computer Simulation of the Substorm of 19 September 1976

5. TYPE OF REPORT & PERIOD COVERED: Scientific Report No. 1

6. PERFORMING ORG. REPORT NUMBER

7. AUTHOR(s): M. Harel, R. A. Wolf, P. H. Reiff and M. Smiddy

8. CONTRACT OR GRANT NUMBER(s): F19628-77-C-0005

9. PERFORMING ORGANIZATION NAME AND ADDRESS
William Marsh Rice University
6100 South Main Street
Houston, Texas 77005

10. PROGRAM ELEMENT, PROJECT, TASK AREA & WORK UNIT NUMBERS
61102F
2311G1AH
G1

11. CONTROLLING OFFICE NAME AND ADDRESS
Air Force Geophysics Laboratory
Hanscom AFB, Massachusetts 01731
Contract Monitor: Capt. David Hardy (PHG)

12. REPORT DATE
7 February 1979

13. NUMBER OF PAGES
24

14. MONITORING AGENCY NAME & ADDRESS (if different from Controlling Office)
28p.

15. SECURITY CLASS. (of this report)
Unclassified

15a. DECLASSIFICATION/DOWNGRADING SCHEDULE

16. DISTRIBUTION STATEMENT (of this Report)
Approved for public release; distribution unlimited.

17. DISTRIBUTION STATEMENT (of the abstract entered in Block 20, if different from Report)

18. SUPPLEMENTARY NOTES

19. KEY WORDS (Continue on reverse side if necessary and identify by block number)
Magnetosphere
Ionosphere
Substorm
Ring Current
Electric Fields

20. ABSTRACT (Continue on reverse side if necessary and identify by block number)
~~We have completed and analyzed~~ several computer runs simulating the behavior of the inner magnetosphere during a substorm-type event that occurred on 19 September 1976, have been completed and analyzed.

~~Our~~ The computer model simulates many aspects of the behavior of the closed-field-line portion of the earth's magnetosphere, and the auroral and subauroral ionosphere. For these regions, the program self-consistently computes electric fields, electric currents, hot-plasma densities, plasma velocities and other

CONT'D

DD FORM 1473 EDITION OF 1 NOV 65 IS OBSOLETE

408 798

parameters.

We present here some highlights of the results of our event simulation. Predicted electric fields for several times during the event agree reasonably well with corresponding data from satellite S3-2. Detailed discussion is presented for a case of rapid subauroral flow that was observed on one S3-2 pass and is predicted by our computer runs. Our computed global distribution of Birkeland current agrees reasonably well with the observations of Iijima and Potemra. In the simulated substorm-type event, plasma-sheet ions are injected earthward of synchronous orbit near midnight and drift westward, forming a ring half-way around the earth by the end of the simulation, 3 hours after substorm onset. The dispersion of ion energies on the dusk side near synchronous orbit has the form commonly observed by McIlwain and collaborators. It appears that the ions would form a complete ring if the simulation were continued for several more hours.

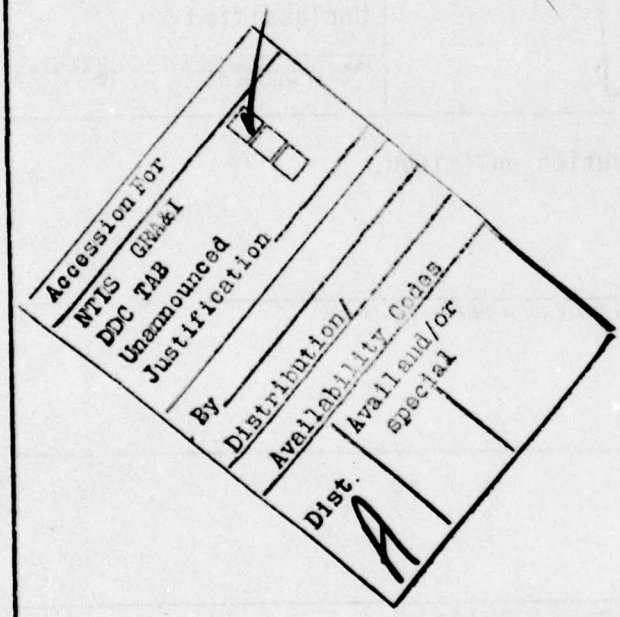

Introduction

There has been a longstanding effort at Rice aimed at accurate computer modeling of the earth's inner magnetosphere. Our most recent work is aimed at simulating a specific observed event, using some observations as input to the model and using other observations as tests of model predictions.

In this paper, we shall present some results of our first attempts to model an event, specifically the substorm-type event that had its onset at about 1000 UT on 19 September 1976. This particular substorm was chosen for its "clean" character and wealth of data usable both for input and model testing (Harel et al., 1977). Given certain initial and boundary conditions, the program self-consistently computes electric fields and plasma flow velocities in the ionosphere and equatorial plane, horizontal ionospheric and field-aligned (Birkeland) currents, temperatures and densities of magnetospheric plasma-sheet plasma and other parameters. In this brief paper, we cannot discuss the time histories of all of these parameters through the event. Instead, we present here just some highlights of the results. A much more detailed account will be presented in future papers.

The present paper is the latest in a long series of efforts at self-consistent calculation of electric fields and plasma flows in the coupled magnetosphere-ionosphere system (e.g., Karlson, 1963, 1971; Fejer, 1964; Block, 1966; Vasyliunas, 1970, 1972; Swift, 1971; Mal'tsev, 1974; Wolf, 1970; Jaggi and Wolf, 1973; Wolf, 1974; Harel and Wolf, 1976). This work has gradually progressed over the years to include more physical processes and more realistic boundary conditions. In the last few years, some progress has also been made by attacking the ionospheric and magnetospheric portions of the problem separately. Many detailed ionospheric-current and electric-field distributions have been computed assuming, as input, the distributions of ionospheric conductivities and Birkeland currents (Yasuhara and Akasofu, 1977; Nopper and Carovillano, 1978, 1979; Nisbet et al., 1978; Kamide and Matsushita, 1978). Analogously, the injection of ring-current particles has been studied extensively using assumed, though often time-variable, electric fields; these electric fields have been estimated using semiempirical formulas based on data sets of various kinds and for various time periods (e.g., McIlwain, 1974; Roederer and Hones, 1974; Konradi et al., 1976; Cowley, 1976; Kivelson, 1976; Ejiri et al., 1977, 1978). Our approach has the disadvantage of being more complicated and cumbersome than these alternatives, but it has several advantages. Namely, it includes more physics and fewer questionable boundary conditions, and it potentially can provide a comprehensive view of both ionospheric and magnetospheric aspects of an observed event.

Assumptions and Logic

We attempt to model only the inner magnetosphere, specifically the region where magnetic field lines are certainly closed, available magnetic-field models can be applied with some confidence and plasma-sheet polarization currents are negligible compared with currents due to gradient and curvature drifts. The dynamics of the outer magnetosphere is extremely complicated, and too poorly understood at present for the kind of detailed quantitative modeling that we are attempting. Our choice of modeling region implies an awkward boundary condition, at the boundary between the inner and outer magnetosphere. However, this choice of region allows us to build reasonable models without impractical computing requirements.

Figure 1 shows the basic logic diagram of our model. The basic logical loop (the central pentagon of the figure) is a modification of a diagram given by Vasyliunas (1970).

Let us briefly discuss the diagram, starting with the box labelled "Hot-Particle Distribution." Using a magnetic-field model and assuming isotropic pitch-angle distributions, we can compute gradient-and-curvature drift currents in the magnetosphere. Our magnetic-field model is an Olson-Pfitzer (1974) analytic model, but including, in addition, the effects of a time-dependent substorm-current loop. This current loop, including an eastward perturbation current across the tail, a westward electrojet, and connecting Birkeland currents, is a modification of one proposed by McPherron et al. (1973); its current strength was adjusted as suggested by midlatitude magnetograms for the event.

Continuing counterclockwise around the central logical loop in Figure 1, we compute Birkeland-current strengths from the divergence of the magnetospheric gradient-and-curvature-drift currents, since the magnetization current, while large, is divergence free. Given the Birkeland-current strength, mapped down to the ionosphere, our next step is to derive the potential distribution in the ionosphere. However, to do this, we need two more pieces of input:

(1) the cross-polar-cap potential drop: from S3-2 electric-field data we estimate the potential drop, and assume a simple distribution (basically, a uniform dawn-dusk electric field with a noontime enhancement) at the high-latitude boundary of our calculation; this boundary lies just equatorward of the electric-field-reversal region;

(2) the distribution of ionospheric conductivity: our model Pedersen and Hall conductivities consist of time-dependent terms that include the day-night asymmetry and solar-zenith-angle effect, and a time-dependent term that gives a rough approximation to the auroral conductivity enhancement; in this latter term, the amount of enhancement is adjusted as a function of time in an effort to be consistent with electron fluxes observed from S3-2.

The condition of current conservation in the ionosphere then becomes an elliptic equation in two dimensions, which is solved numerically, given the potential distribution at the polar-cap boundary as one boundary condition and a condition of no current across the low-latitude boundary, which is at approximately 21 degrees geomagnetic latitude.

We map the ionospheric potential distribution out along field lines to the equatorial plane, assuming no field-aligned electric fields, but adding on the induction electric field, to get the total magnetospheric electric field.

We now compute the total drift velocities ($\underset{\sim}{E} \times \underset{\sim}{B}$, gradient and curvature) of magnetospheric ions and electrons of various energies. Specifically, we compute the motions of the inner edges of plasma-sheet electrons of 5 energies, and ions of 11 energies, each inner edge being represented by approximately 18 independently computed points. The boundary positions are advanced by an amount corresponding to multiplying the computed velocities by the time step Δt. In computing electron boundary positions, we also include, in an approximate way, the effect of loss by precipitation. For simplicity in these initial model calculations, electrons near the inner edge of the plasma sheet are assumed to be lost by simple strong-pitch-angle scattering, as suggested by Vasyliunas (1968) and Kennel (1969).

The program goes completely around this logical loop every time step, which is typically 30 seconds magnetosphere time.

Figure 2 illustrates some aspects of the event being simulated, which might variously be described as a very long substorm, a quick succession of several short substorms or a substorm followed by a "convection-driven negative bay" (Pytte et al., 1978). The lower panel shows cross-polar-cap potential drops as estimated from S3-2 data. Note that this substorm-type event is associated with an increase in the polar-cap potential drop, an association previously suggested by Mozer (1973). Note also that the potential drop continued to rise after substorm onset, which might account for the prolonged negative bay (Pytte et al., 1978).

Results

We briefly present here a few highlights of our results, emphasizing some aspects that have been directly compared with observations.

We must emphasize that we are presenting a comparison of observed data with results of our first tries at computer simulating an observed magnetospheric event. Some data were used as input as described in Section II, to help us determine the polar-cap boundary, the cross-polar-cap potential drop, the conductivity and the magnetic-field model, but data were not used in any other significant way. Given the available input data, there is still some flexibility in the boundary conditions, and we could adjust the boundary conditions in various respects to improve agreement with data, but we have not done that yet. Presented below are our first tries at computer simulating the event, with no effort at optimizing the fit.

We have actually done four computer runs, as indicated in Table 1. Run #3 was done with a time-independent magnetic-field model, to isolate the effects of the induction electric field on ring-current injection. The runs also involved two different degrees of latitudinal smoothing of conductivities. (The reason for smoothing of the conductivities is that the difference equation that we use to conserve current in the ionosphere becomes an inaccurate

approximation to the differential equation when there are sharp jumps in conductivity. Run #1 involved about as sharp a conductivity gradient as we can handle accurately with the present 21 x 28 grid and present numerical method.) Except for the dotted and dashed curves in Figure 6, all results presented here are for Run #4.

Figures 3-5 show observations vs. theory for the three passes of S3-2 that occurred during the event, before 1300 UT, when the simulation ended. The top two panels of each figure show observed and predicted electric fields. The lower panel shows predicted Birkeland currents. (S3-2 magnetometer data for this date are not reduced yet.) The dotted portion of the top panel represents the polar-cap-and-boundary-layer electric field, which we do not model. However, the input polar-cap potential drop is computed essentially from the area under the dotted curve. The boundary of our calculation (the poleward edge of the computed electric fields), is adjusted in Figures 3-6 (but not Figure 7) to correspond to the observed boundary of the polar-cap-and-boundary-layer region (boundary between dotted and solid observation curves).

We would like to make three general comments concerning the comparison between observed and predicted electric fields in Figures 3-5.

(1) There is little agreement between data and theory with regard to small details, perhaps due to the fact that the model conductivity distribution is smooth and undetailed.

(2) Both data and theory agree that the region below about 60 degrees invariant latitude is rather well shielded from the high-latitude convection field, even in this time-dependent situation. The greatest leakage through the shielding occurred, both in the data and the theory, on the outbound part of pass 4079A South, just after substorm onset. In the model, auroral conductivities were increased suddenly at onset, and the ring current had not had time to rearrange itself completely to restore strong shielding.

(3) Electric fields on the dawn side generally tend to decline smoothly with decreasing latitude, both in the theory and the data, but the same is not true on the dusk side, where, particularly past 1800 local time, the strongest poleward electric field generally tends to occur well equatorward of the polar-cap boundary. Furthermore, in both the model and S3-2 electric-field data, electric fields below the polar-cap boundary tend to be larger on the dusk side than on the dawn side, an effect previously noticed by Kelley (1976). Our models essentially always show greater potential drops at dusk than at dawn -- a result of Hall currents flowing antisunward across the conductivity jumps at dawn and dusk (Wolf, 1970).

Rapid Subauroral Flow

The most striking feature of the data shown in Figures 3-5 is the sharp electric-field peak observed well below the polar-cap boundary in the last half of orbit 4079B-South (Figure 5). We shall refer to this feature as "rapid subauroral flow." Data from the same auroral-zone pass is shown in more detail in Figure 6 (top panel).

Panels 2-4 display curves for runs 1 (dotted), 2 (dashed), and 4 (solid). Run 3 results are generally similar to run 2 and will not be discussed here.

The second panel of Figure 6 shows calculated electric fields, in a form that displays all the fine structure available in the model. (Our grid spacing is approximately 1.6° in latitude. However, the program employs a special back-correction scheme that allows it to keep track of effects of Birkeland current on a much finer scale. These fine-scale corrections are included in Figure 6, but not Figures 3-5.)

The third panel of Figure 6 shows predicted Birkeland-current strengths along that trajectory.

Panel 4 displays model values of height-integrated Pedersen conductivities. The model global conductivity includes day-night asymmetry, solar-zenith-angle dependence and electron-precipitation effects. The auroral conductivity enhancement is estimated crudely from observed electron fluxes. For a more detailed discussion, see Harel et al. (1977). Our computer model cannot tolerate very large conductivity gradients, so we had to smooth the conductivity profile to some extent (see panel 4 and also Table 1).

The bottom panel of Figure 6 shows height-integrated Pedersen conductivity, estimated directly from measured electron fluxes using the formula

$$\Sigma_p \text{ (mho)} = 0.5 + 5.2 \times (\text{Electron energy flux})^{1/2} \qquad (1)$$

where the energy flux is in erg cm^{-2} sec^{-1} (Harel et al., 1977). Unfortunately, the geometric factor of the electron detector on S3-2 was too small to allow reliable estimation of the low-latitude edge of the diffuse aurora.

The exciting feature of Figure 6 is, of course, that the computer runs all predicted the observed rapid subauroral flow and at approximately the right location. Similar rapid flows have been observed many times before, often associated with the trough (Heelis et al., 1976; Smiddy et al., 1977; Maynard, 1978; Spiro et al., 1978).

Note that the location of the peak of the rapid subauroral flow computed in run 4 agrees very well with observations, while the other two runs show peaks that lie approximately a degree poleward of the observed one. This difference in model results is easy to understand physically: for runs 1 and 2 we underestimated the polar-cap potential drop; consequently the plasma-sheet ions were not injected as deep into the magnetosphere as was the case for run 4, and the rapid subauroral flow did not extend to as low latitude (Southwood and Wolf, 1978).

An important feature of our predicted Birkeland currents for this pass (panel 3) is that we get only downward currents. This is different from the observation of an upward current sheet at the poleward edge of one rapid subauroral flow (Smiddy et al., 1977). We attribute this difference to the different local time (2100 MLT) of this earlier measurement. Theoretically, only a single current sheet is needed to account for the peak electric field in the trough region, provided that the conductivity gradient there is large enough (Southwood and Wolf, 1978). Approximately a factor-of-two increase in Pedersen conductivity is needed between 61° and 62° to be consistent with the sharp decline of the observed electric field in that region. The data are not inconsistent with such an increase. Also, the conductivity model with the sharpest gradient (dotted curve) gives rise to the sharpest calculated electric-field peak, as expected.

Our computer model often shows rapid subauroral flows in the dusk-to-midnight sector, though not elsewhere, which is consistent with the previously mentioned observations. We should mention that no other clear rapid subauroral flows were observed during this simulated event, and none are predicted by the model for the S3-2 satellite paths, with the following partial exception: one of the computer runs indicated an electric field on pass 4079A South that peaked at about 42 mV/m and had a shape that would classify it as a marginal case of rapid subauroral flow. The observations indicate, for that case, a complicated structure rather than a clear rapid-subauroral-flow signature.

We should also acknowledge a different and conflicting interpretation of rapid subauroral flows (Mozer, 1978), an interpretation in terms of field-aligned potential drops between relevant satellite atltitudes (250-1500 km) and the lower ionosphere.

Birkeland-Current Patterns

Figure 7 compares our computed distribution of Birkeland currents with a summary of active-period observations by Iijima and Potemra (1978). The general pattern of computed currents did not vary much with time through the substorm, although, of course, the low-latitude boundary of the currents moved equatorward during the event, and the current strengths increased. The poleward set of Birkeland currents (region 1 currents in the nomenclature of Iijima and Potemra) are poleward of our modeled region. We estimate their distribution very roughly by calculating the currents into our poleward boundary and assuming that those currents flow directly out along field lines from there. The thickness shown for the computed region 1 currents in Figure 7 is arbitrary.

The observed and predicted patterns agree in their general sense, which is not surprising, since convection theories (Schield et al., 1969; Wolf, 1974) predicted the basic pattern before it was observed, and it has been a consistent feature of our computer models. An encouraging feature of the comparison in Figure 7 is the triple-current-sheet region that exists near midnight in both the Triad observations and the theory. (Starting from the polèward boundary and moving toward the equator, we have downward, upward, and then downward currents). The model current structure appears to be rotated about two hours later in local time, as compared to the observations. We suspect that this feature of the model could be brought into agreement with observations by a minor adjustment of the boundary potential at the polar cap.

In the models, we do see multiple reversals of Birkeland currents around local midnight, but we do not see them near dusk. Thus the models always indicate a predominantly downward current in the region of rapid subauroral flow at dusk. On the other hand, Figure 7 predicts Birkeland-current reversals at low latitude near midnight, which may correspond to the effect observed by Smiddy et al. (1977).

Ring-Current Injection

For this simulation, the initial distribution of plasma-sheet particles ("initial" meaning 0900UT on 19 September 1976) was taken to be a configuration corresponding to near-equilibrium for a 20 kV potential drop. The initial plasma sheet was taken to have Maxwellian velocity distributions and uniform flux-tube content antiearthward of the inner-edge region. At L = 10, the density and temperature parameters correspond to $n_i=n_e \approx 1.5$ cm^{-3}, $T_e=1.5$ keV, $T_i=4.5$ keV. There was assumed to be no quiet-time ring current of particles circling the earth on closed orbits. (For more details on the initial condition, and technical details of the approach, see Harel et al., 1977).

Starting from this initial condition, and assuming constant total-flux-tube content for flux tubes convecting earthward from the outer boundary of the calculation, we let the particle distribution evolve in the self-consistently computed electric field.

Figure 8 gives ones view of the time-evolution of the ring current. Namely, it shows what plasma-sheet ions a satellite at L=6.6, at dusk, would have seen, according to our simulation. Note that the higher energies arrived first, followed by the lower energies. Eventually essentially the entire plasma-sheet ion population would engulf a spacecraft at synchronous orbit at dusk. Unfortunately, there was no satellite at geosynchronous orbit near local dusk in the case of the simulated event, but we are encouraged by the fact that the predicted ion dispersion curve resembles a type of pattern often observed by McIlwain and collaborators.

The left diagram in Figure 9 shows the inner edge of the plasma sheet at the end of our simulation run, three hours after substorm onset. The injected ring current has almost reached local noon. A numerical problem with the present version of the simulation program has prevented us from following the injection past local noon, but the computed velocities make it clear that ring formation will continue approximately as shown in the right half of Fig. 9.

Various other modeling efforts (e.g., McIlwain, 1974; Roederer and Hones, 1974; Smith et al., 1979) have produced realistic-looking dispersion curves and/or ring formations. These efforts are, however, all open to the objection that the electric fields and ring current are not computed self-consistently, considering the fact that the structure of the ring current strongly affects the electric-field distribution. We do the calculation self-consistently, and we indeed find that the ring current does strongly affect the electric-field pattern near its own inner edge, as shown in Figure 10; these gradients change substantially as the ring current evolves.) Nevertheless, even with this major complication included, the enhanced convection electric field has automatically injected a realistic ring current in our simulated event.

The positive results of these increasingly sophisticated modeling efforts constitute a verification of the idea that the ring current is injected into the inner magnetosphere mainly by time-dependent enhancement of the convection electric field and consequent adiabatic particle acceleration, rather than by nonadiabatic acceleration of cold particles to kilovolt energies at the inner edge of the ring current. Of course, a far more definitive test will occur when we model a magnetic storm, for which particle data are available from both the tail plasma sheet and the ring current, and when we include an initial quiet-time ring current self-consistently in the model.

Summary

We have displayed some highlights of results of our first attempt at simulating an observed magnetospheric event. Comparison with observations has come out remarkably well, particularly considering that, in these first tries, we have not adjusted any boundary conditions or assumptions to improve agreement with the data. Of course, much work remains to be done to include more physics in the models and to model more and different events.

Acknowledgments. We are grateful to Ameen Ahmad, H. Kent Hills, Janice Karty, and Robert Spiro for their work in displaying model results, to W. J. Burke, D. A. Hardy and F. J. Rich for their efforts in reducing data from the S3-2 satellite, and to Robert Spiro for several illuminating discussions and for helpful comments on the manuscript.

This report is essentially a combination of parts of two papers that have been submitted for publication, namely the following:

Harel, M., R. A. Wolf, P. H. Reiff and M. Smiddy, Computer modeling of events in the inner magnetosphere, to be published in Quantitative Modeling of Magnetospheric Processes, Geophys. Monogr. Ser., Vol. 21, edited by W. P. Olson, AGU, Washington, D.C., 1979.

Wolf, R. A., and M. Harel, Magnetospheric plasma dynamics, submitted for publication in Astrophysics and Space Library Series, covering the Chapman Conference on Magnetospheric Substorms and Related Plasma Processes.

The work reported here was suppported mainly by Air Force Contract F19628-77-C-0005. However, the portion dealing with analysis and interpretation of data from satellite S3-2 was supported primarily by Air Force Contract F19628-78-C-0078, and to a lesser extent by NASA grants NGR44-006-137 and NGL44-006-012. Development of the basic computer program used was supported substantially by NSF grant ATM74-21185.

References

Block, L. P., On the distribution of electric fields in the magnetosphere, J. Geophys. Res., 71, 855, 1966.

Cowley, S. W. H., Energy transport and diffusion, in Physics of Solar Planetary Environments, ed. D. J. Williams, Amer. Geophys Un., Washington, D.C., p. 582, 1976.

DeForest, S. E., and C. E. McIlwain, Plasma clouds in the magnetosphere, J. Geophys. Res. 76, 3587, 1971.

Ejiri, M., R. A. Hoffman and P. H. Smith, Energetic particle penetrations into the inner magnetosphere, Goddard Space Flight Center Report X-625-77-254, 1977

Ejiri, M., R. A. Hoffman and P. H. Smith, The convection electric field model for the magnetosphere based on Explorer 45 observations, J. Geophys. Res., 83, 4811, 1978

Fejer, J.A., Theory of geomagnetic daily disturbance variations, J. Geophys. Res., 69, 123, 1964.

Harel, M., and R. A. Wolf, Convection, in Physics of Solar-Planetary Environments, Vol. II, edited by D. J. Williams, Amer. Geophys. Un., Washington, D. C., p. 617, 1976.

Harel, M., R. A. Wolf, P. H. Reiff and H. K. Hills, Study of plasma near the earth's plasmapause, U.S. Air Force Geophysics Laboratory Report AFGL - TR-77-0286, 1977.

Heelis, R. A., R. W. Spiro, W. B. Hanson and J. L. Burch, Magnetosphere-ionosphere coupling in the mid-latitude trough, Trans. Am. Geophys. Union, 57, 990, 1976.

Iijima, T., and T. A. Potemra, Large-scale characteristics of field-aligned currents associated with substorms, J. Geophys. Res., 83, 599, 1978.

Jaggi, R. K., and R. A. Wolf, Self-consistent calculation of the motion of a sheet of ions in the magnetosphere, J. Geophys. Res., 78, 2852, 1973.

Kamide, Y. and S. Matsushita, Simulation studies of ionospheric electric fields and currents in relation to field-aligned currents. 1. Quiet periods, submitted to J. Geophys. Res., 1978.

Karlson, E. T., Streaming of plasma through a magnetic dipole field, Phys. Fluids, 6, 708, 1963.

Karlson, E. T., Plasma flow in the magnetosphere. I. A two-dimensional model of stationary flow, Cosm. Electrodyn., 1, 474, 1971.

Kelley, M. C., Evidence that auroral-zone electric fields act in opposition to super-rotation of the upper atmosphere, Planet Space Sci., 24, 355, 1976.

Kennel, C. F., Consequences of a magnetospheric plasma, Rev. Geophys. 7, 379, 1969.

Kivelson, M. G., Magnetospheric electric fields and their variation with geomagnetic activity, Rev. Geophys. Space Phys., 14, 189, 1976.

Konradi, A., C. L. Semar, and T. A. Fritz, Injection boundary dynamics during a geomagnetic storm, J. Geophys. Res., 81, 3851, 1976.

Mal'tsev, Yu. P., The effect of ionospheric conductivity on the convection system in the magnetosphere, Geomag. Aeron., 4, 128, 1974.

Maynard, N. C., On large poleward-directed electric fields at sub-auroral latitudes, Geophys. Res. Lett., 5, 617, 1978.

McIlwain, C. E., Substorm injection boundaries, in Magnetospheric Physics, edited by B. M. McCormac, D. Reidel, Dordrecht-Holland, p. 143, 1974.

McPherron, R. L., C. T. Russell and M. P. Aubry, Satellite studies of magnetospheric substorms on August 15, 1968. 9. Phenomenological model of substorms, J. Geophys. Res., 78, 3131, 1973.

Mozer, F. S., On the relationship between the growth and expansion phases of substorms and magnetospheric convection, J. Geophys. Res., 78, 1719, 1973.

Mozer, F. S., Implications of S3-3 and ISEE electric field data on models of magnetospheric electric fields, paper presented at the Chapman Conference on Quantitative Modeling of Magnetospheric Processes, La Jolla, Ca., 1978.

Nisbet, J. S., M. J. Miller and L. A. Carpenter, Currents and electric fields in the ionosphere due to field-aligned auroral currents, J. Geophys Res., 83, 2647, 1978.

Nopper, R. W. Jr., and R. L. Carovillano, Polar equatorial coupling during magnetically active periods, Geophys. Res. Lett., 5, 699, 1978.

Nopper, R. W. Jr., and R. L. Carovillano, Ionospheric electric fields driven by field-aligned currents, in Quantitative Modeling of the Magnetospheric Processes, Geophys. Monogr. Soc., Vol. 21, edited by W. P. Olson, AGU, Washington, D. C., 1979.

Olson, W. P., and K. A. Pfitzer, A quantitative model of the magnetospheric magnetic field, J. Geophys. Res., 79, 3739, 1974.

Pytte, T. R., R. L. McPherron, E. W. Hones, Jr., and H. I. West, Jr., Multiple-satellite studies of magnetospheric substorms: distinction between polar magnetic substorms and convection-driven negative bays, J. Geophys. Res., 83, 663, 1978.

Roederer, J. G., and E. W. Hones, Jr., Motion of magnetospheric particle clouds in a time-dependent electric field model, J. Geophys. Res., 79, 1432, 1974.

Schield, M. A., J. W. Freeman, and A. J. Dessler, A source for field-aligned currents at auroral latitiudes, J. Geophys. Res., 74, 247, 1969.

Smiddy, M., M. Kelley, W. Burke, F. Rich, R. S. Sagalyn, B. Schumann, R. Hays and S. Lai, Intense poleward-directed electric fields near the ionospheric projection of the plasmapause, Geophys. Res. Lett., 4, 543, 1977.

Smith, P. H., H. K. Bewtra and R. A. Hoffman, Motions of charged particles in the magnetosphere under the influence of a time-varying large-scale convection electric field, in Quantitative Modeling of the Magnetospheric Processes, Geophys Monogr. Ser., vol. 21. edited by W. P. Olson, AGU, Washington, D.C., 1979.

Southwood, D. J., and R. A. Wolf, An assessment of the role of precipitation in magnetospheric convection, J. Geophys Res., 83, 5227, 1978.

Spiro, R. W., R. A. Heelis and W. B. Hanson, Ion convection and the formation of the midlatitude F-region ionospheric trough, J. Geophys. Res., 83, 4255, 1978.

Swift, D. W., Possible mechanisms for formation of the ring current belt, J. Geophys. Res., 76, 2276, 1971.

Vasyliunas, V. M., A mathematical model of plasma motions in the magnetosphere, Trans. Am. Geophys. Un., 49, 232, 1968.

Vasyliunas, V. M., Mathematical models of magnetospheric convection and its coupling to the ionosphere, in Particles and Fields in the Magnetosphere, edited by B. M. McCormac, D. Reidel, Dordrecht-Holland, p. 60, 1970.

Vasyliunas, V. M., The interrelationship of magnetospheric processes, in Earth's Magnetospheric Processes, edited by B. M. McCormac, D. Reidel, Dordrecht-Holland, p. 29, 1972.

Wolf, R. A., Effects of ionospheric conductivity on convective flow of plasma in the magnetosphere, J. Geophys. Res., 75, 4677, 1970.

Wolf, R. A., Calculations of magnetospheric electric fields, in Magnetospheric Physics, edited by B. M. McCormac, D. Reidel, Dordrecht-Holland, p. 167, 1974.

Yasuhara, F. and S. -I. Akasofu, Field-aligned currents and ionospheric electric fields, J. Geophys. Res., 82, 1279, 1977.

Table 1. Computer-Simulation Runs

Computer Run	Peak Polar-Cap Potential Drop	Conductivity Model	Induction Electron Field
1	80 kV	Minimum smoothing	Yes
2	80 kV	Greater smoothing	Yes
3	80 kV	Greater smoothing	No
4	140 kV	Greater smoothing	Yes

Figure Captions

Fig. 1. Overall logic diagram for our program. The central pentagon represents the main computational loop, executed every time step. The rectangles that appear at the corners of the pentagon represent basic parameters computed. Input data are indicated by curly brackets. Subsidiary models, used as input to the main program, are indicated by rectangles with rounded corners. Dashed lines indicate features that we plan to include in the program but have not included yet

Fig. 2. Fort Churchill H-magnetogram and polar-cap potential drop for 19 September 1976. The lower panel shows polar-cap potential drops estimated from S3-2 electric-field data. Sizes of boxes are indicative of estimated errors. The solid curve shows the potential drop assumed in the simulation. Electric-field data from the 1140 UT pass arrived later than those from the other passes, and as a result some simulation runs followed the dashed line from 1040 to 1300 UT.

Fig. 3. Data and theory for the 1000 UT pass of satellite S3-2. The top panel shows data from the AFGL electric field instrument. We have plotted the forward component of $\underset{\sim}{E}$, i.e., the component in the direction of satellite motion. The dotted section of the curve is the polar-cap-and-boundary-layer region, which we do not model. The second panel shows the corresponding component of the theoretically predicted electric field at the satellite's location (latitude, longitude and altitude) for the universal times in question. The bottom panel shows predicted Birkeland-current strength (positive values mean upward current). The legend gives Greenwich Mean Time, magnetic local time and invariant latitude. Satellite altitude ranges from 1025 km to 1375 km.

Fig. 4. Data and theory for the 1050 UT pass of S3-2. The format is the same as Figure 3. Satellite altitude ranges from 800 km to 260 km.

Fig. 5. Data and theory for 1150 UT pass of S3-2. The format is the same as Figure 3. Satellite altitude ranges from 1000 km to 1360 km.

Fig. 6. Detailed view of the dusk-auroral-zone pass for the southern part of orbit 4079B of satellite S3-2. The top panel shows the observed electric-field component opposite to satellite motion (approximately the poleward component). The second panel gives essentially the same component of the theoretical-model electric field. The third panel gives predicted Birkeland currents, and the fourth panel shows the model height-integrated Pedersen conductivities. Solid curves in panels 2-4 pertain to run #4; the dotted and dashed curves correspond to runs 1 and 2. The bottom panel shows conductivities estimated directly from the data using equation (1).

Fig. 7. Comparison of a typical computed Birkeland current pattern (for 1150 UT on 19 September 1976) and an average observed pattern for active times (Iijima and Potemra, 1978).

Fig. 8. Ion arrival times at r = 6.6 R_E, MLT = 1820. Substorm onset was approximately 1000 UT. The solid curve shows the arrival time for ions of various energies at 6.6R_E, MLT = 1820. The dotted line shows what the arrival times would be for ions of various energies that gradient drift in the equatorial plane of a dipole magnetic field, with no electric field. The X's represent energies of the ions that we follow in detail. Specifically, an "X" means that the inner edge for that energy is earthward of 6.6 R_E.

Fig. 9. Diagram a shows the inner edge of the model plasma sheet, for three types of plasma-sheet particles, three hours after onset. The three particle types are ~2 keV electrons, zero thermal-energy particles, and ~50 keV ions. Diagram b shows the way in which the ring current should be expected to continue to wrap up.

Fig. 10. $\underset{\sim}{E} \times \underset{\sim}{B}$ drift velocities in the magnetospheric equatorial plane, at 1300 UT, 3 hours after onset. Note the large gradients in $\underset{\sim}{E} \times \underset{\sim}{B}$ drift near the inner edge.

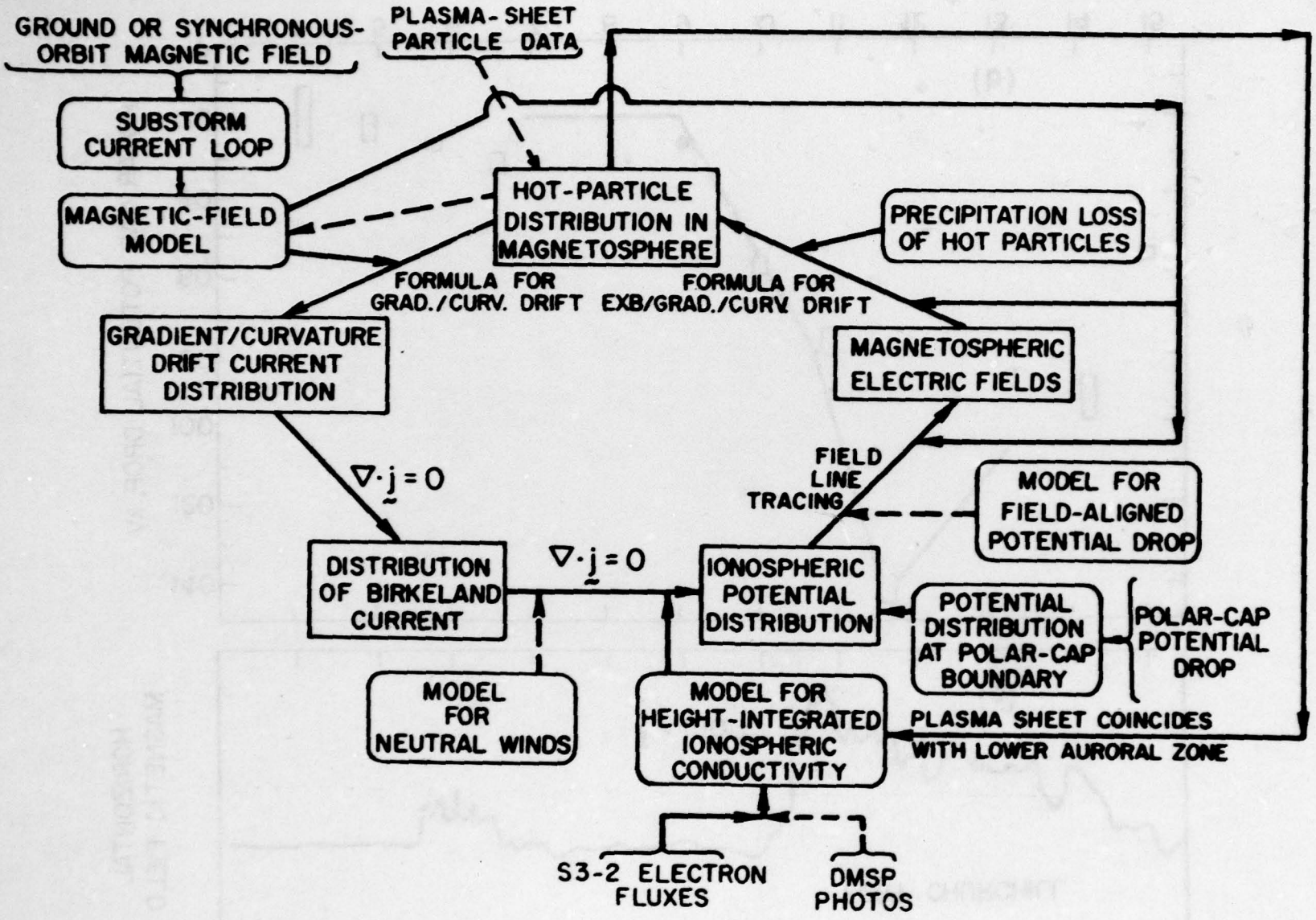
GROUND OR SYNCHRONOUS-ORBIT MAGNETIC FIELD
PLASMA-SHEET PARTICLE DATA
SUBSTORM CURRENT LOOP
MAGNETIC-FIELD MODEL
HOT-PARTICLE DISTRIBUTION IN MAGNETOSPHERE
PRECIPITATION LOSS OF HOT PARTICLES
FORMULA FOR GRAD./CURV. DRIFT
FORMULA FOR EXB/GRAD./CURV. DRIFT
GRADIENT/CURVATURE DRIFT CURRENT DISTRIBUTION
MAGNETOSPHERIC ELECTRIC FIELDS
$\nabla \cdot \underset{\sim}{j} = 0$
FIELD LINE TRACING
MODEL FOR FIELD-ALIGNED POTENTIAL DROP
DISTRIBUTION OF BIRKELAND CURRENT
$\nabla \cdot \underset{\sim}{j} = 0$
IONOSPHERIC POTENTIAL DISTRIBUTION
POTENTIAL DISTRIBUTION AT POLAR-CAP BOUNDARY
POLAR-CAP POTENTIAL DROP
MODEL FOR NEUTRAL WINDS
MODEL FOR HEIGHT-INTEGRATED IONOSPHERIC CONDUCTIVITY
PLASMA SHEET COINCIDES WITH LOWER AURORAL ZONE
S3-2 ELECTRON FLUXES
DMSP PHOTOS

Figure 1

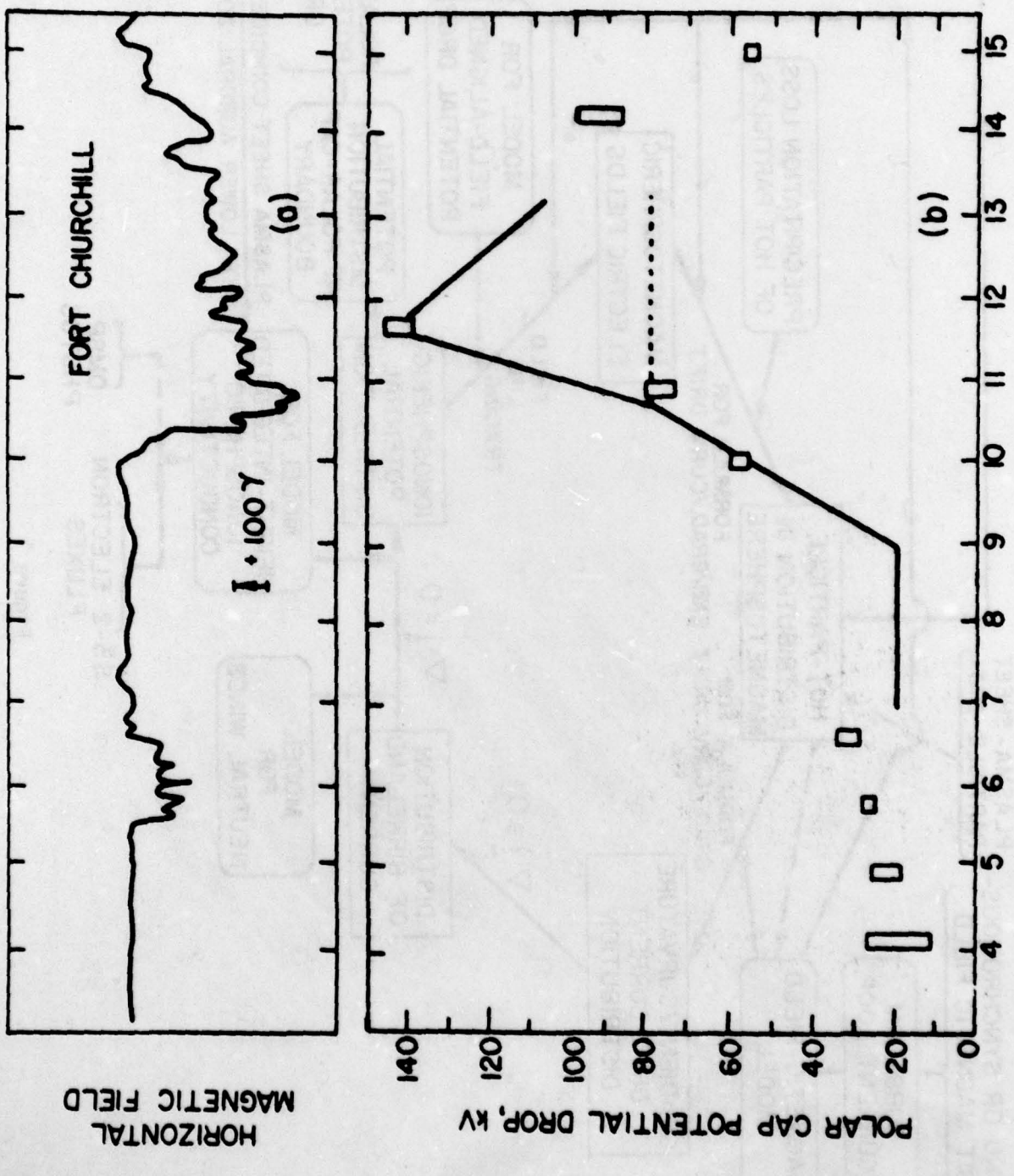
FORT CHURCHILL
(a)
1 · 100γ
HORIZONTAL MAGNETIC FIELD
(b)
POLAR CAP POTENTIAL DROP, kV
0
20
40
60
80
100
120
140
4
5
6
7
8
9
10
11
12
13
14
15
UT

Figure 2

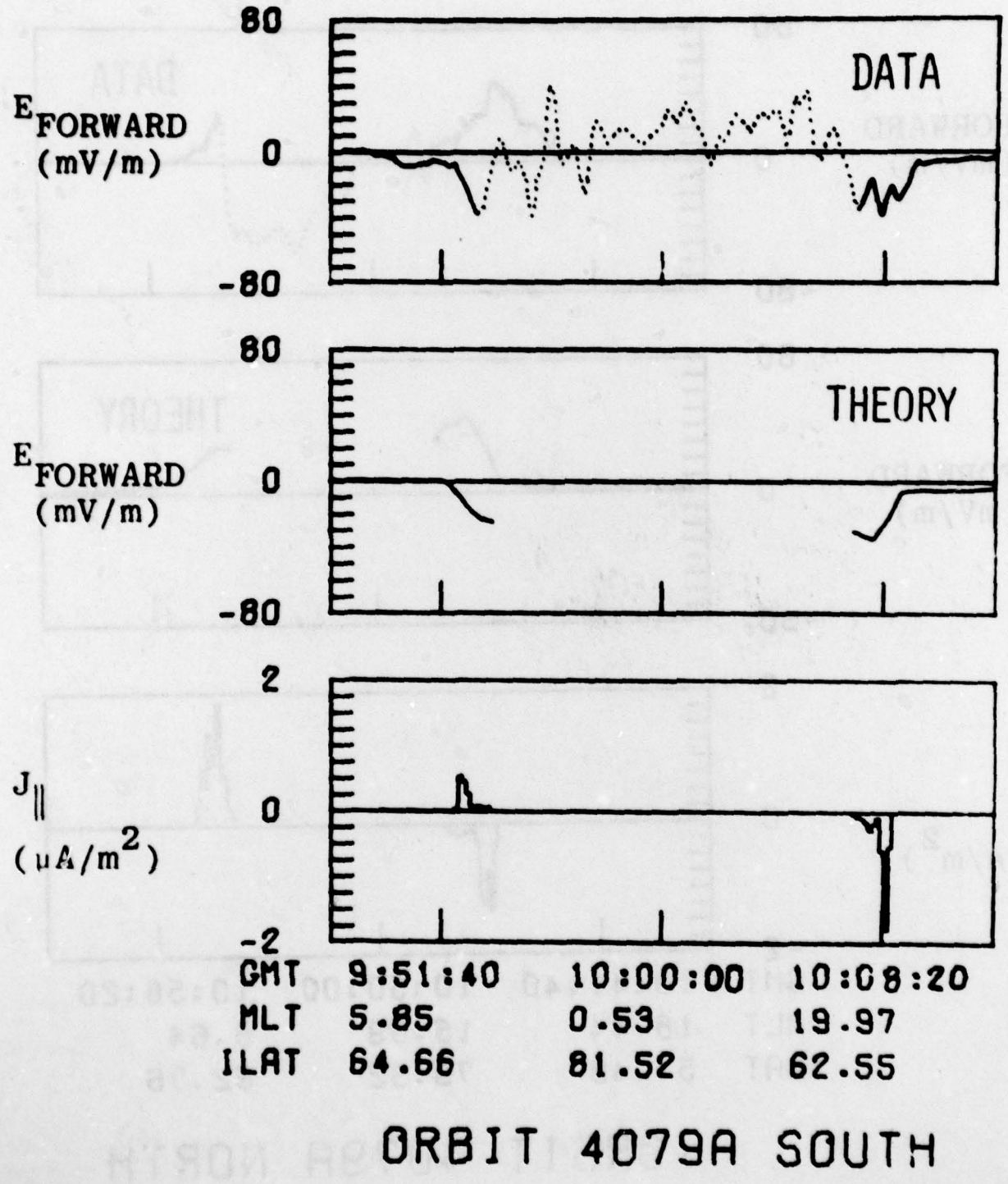
80
$E_{FORWARD}$ (mV/m)
0
-80
DATA
80
$E_{FORWARD}$ (mV/m)
0
-80
THEORY
2
$J_{\parallel}$ ($\mu A/m^2$)
0
-2
GMT 9:51:40 10:00:00 10:08:20
MLT 5.85 0.53 19.97
ILAT 64.66 81.52 62.55
ORBIT 4079A SOUTH

Figure 3

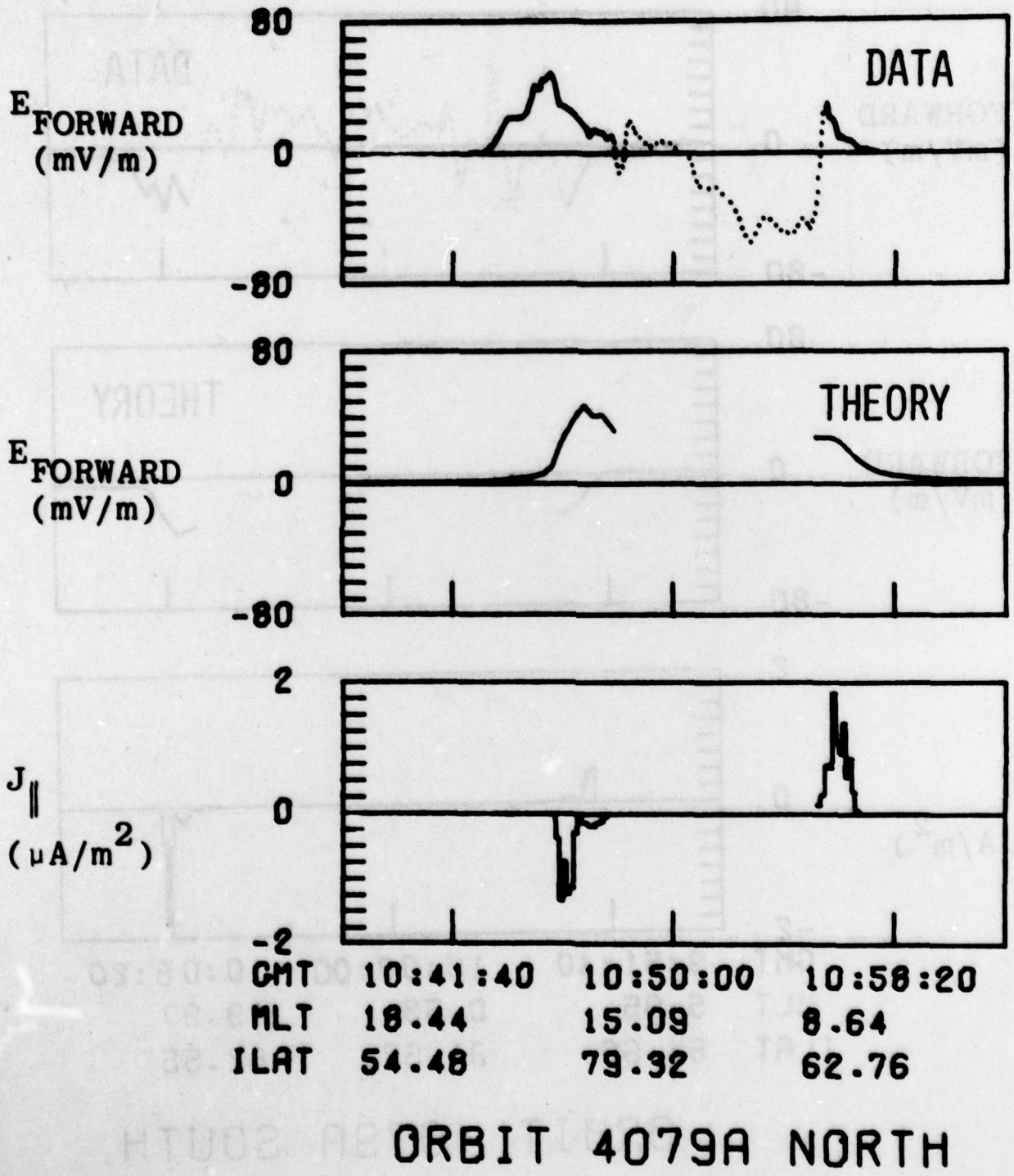
80
$E_{FORWARD}$ (mV/m)
0
-80
DATA
80
$E_{FORWARD}$ (mV/m)
0
-80
THEORY
2
$J_{\parallel}$ ($\mu A/m^2$)
0
-2
GMT 10:41:40 10:50:00 10:58:20
MLT 18.44 15.09 8.64
ILAT 54.48 79.32 62.76
ORBIT 4079A NORTH

Figure 4

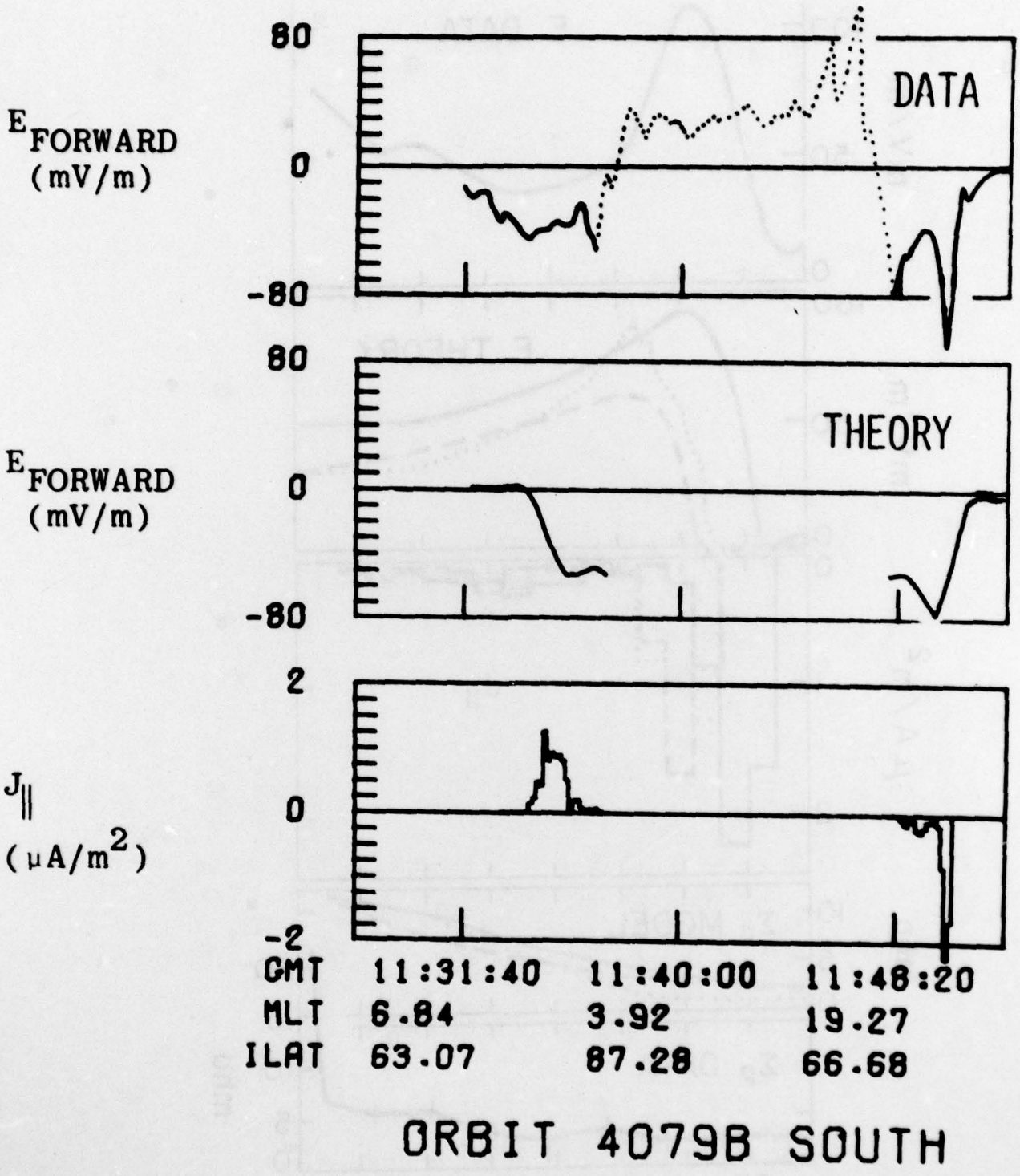
80
0
-80
DATA
$E_{FORWARD}$ (mV/m)
80
0
-80
THEORY
$E_{FORWARD}$ (mV/m)
2
0
-2
$J_{\parallel}$ ($\mu A/m^2$)
GMT 11:31:40 11:40:00 11:48:20
MLT 6.84 3.92 19.27
ILAT 63.07 87.28 66.68
ORBIT 4079B SOUTH

Figure 5

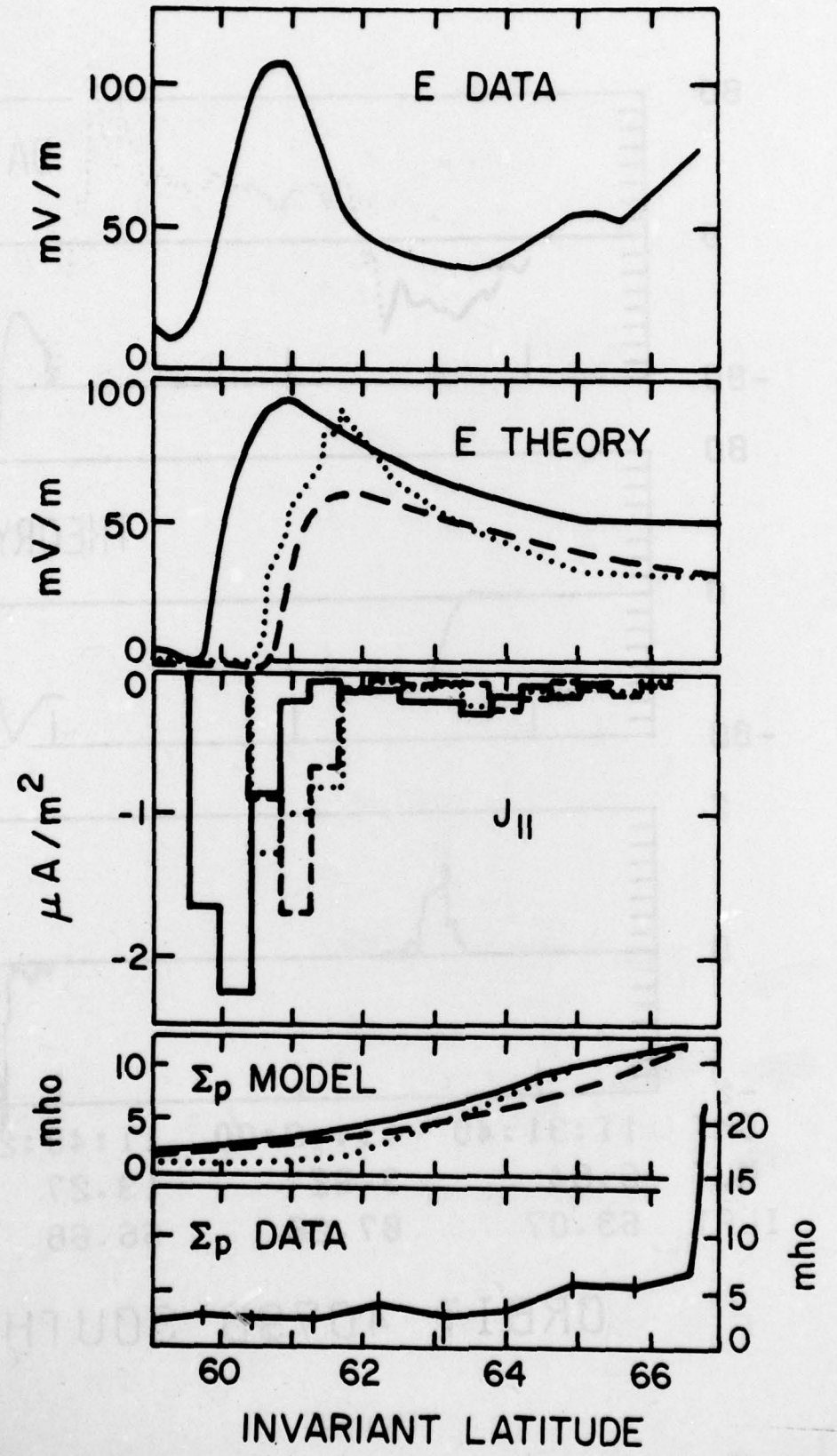
E DATA
100
50
0
mV/m
E THEORY
100
50
0
mV/m
0
-1
-2
μA/m²
J||
mho
10
5
0
Σp MODEL
20
15
10
5
0
Σp DATA
mho
60
62
64
66
INVARIANT LATITUDE

Figure 6

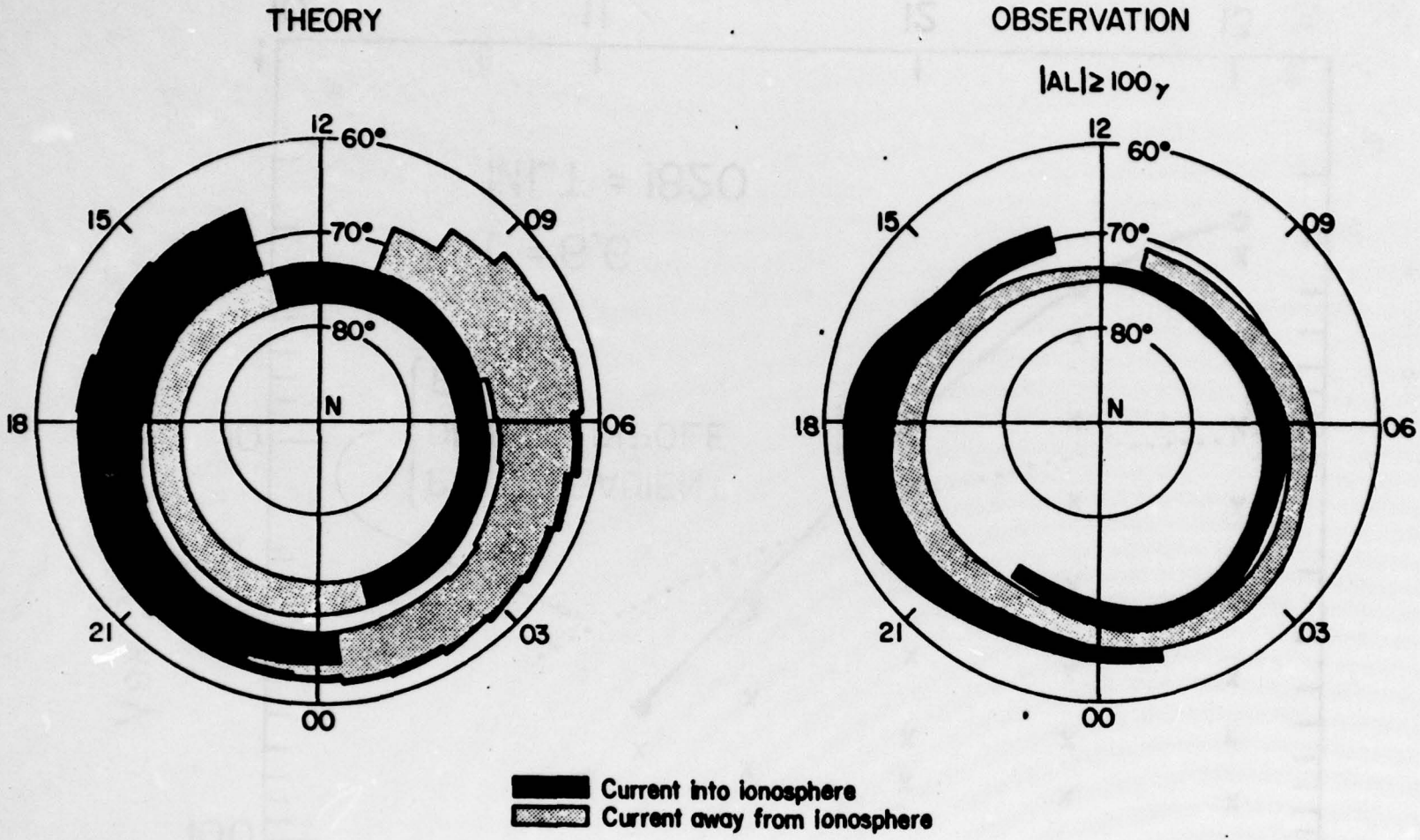
THEORY
OBSERVATION
|AL|≥ 100γ
12
60°
70°
80°
N
09
06
03
00
21
18
15
Current into ionosphere
Current away from ionosphere

Figure 7

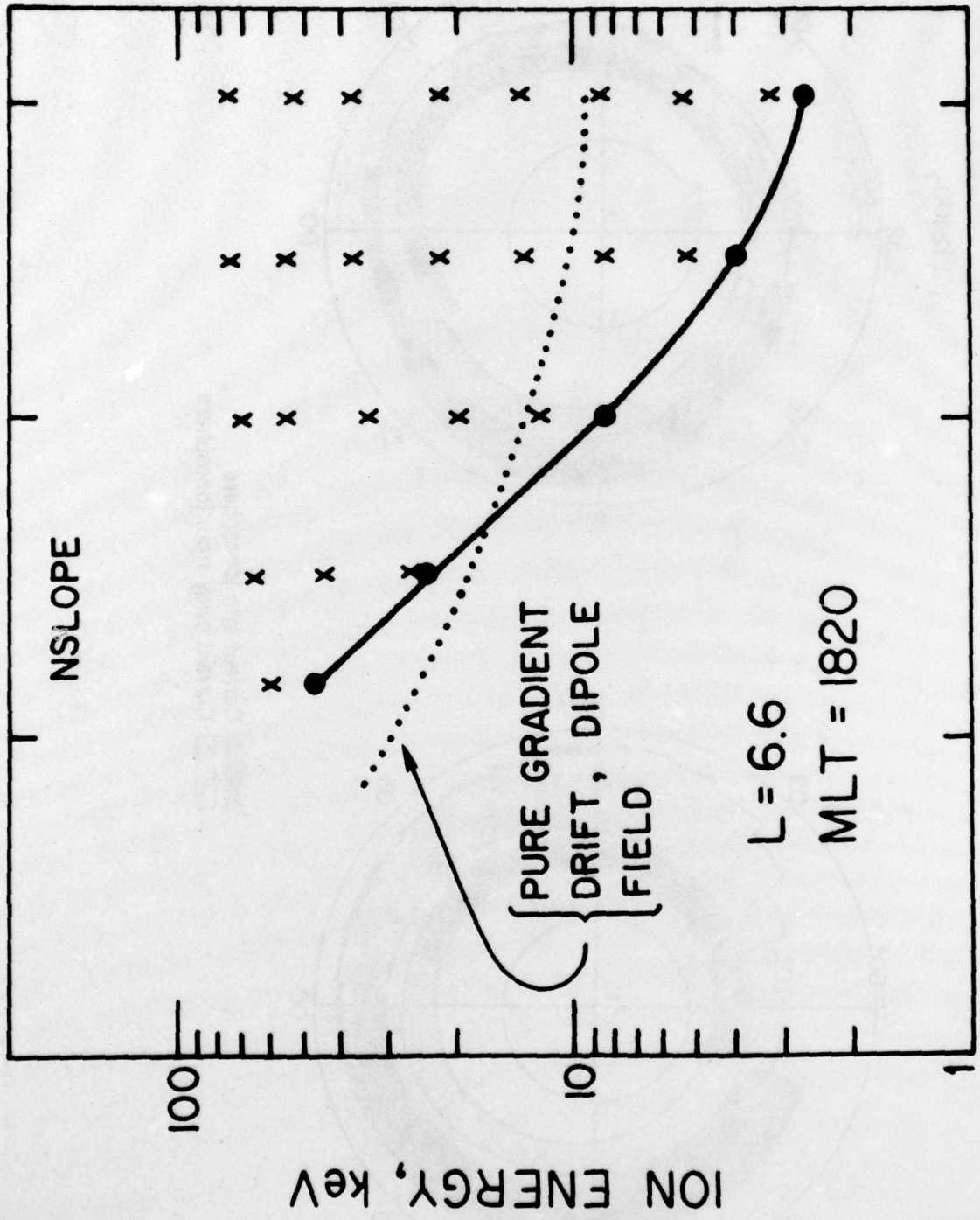
ION ENERGY, keV
100
10
1
NSLOPE
PURE GRADIENT
DRIFT, DIPOLE
FIELD
L=6.6
MLT = 1820
10
11
12
13
UT
ONSET

Figure 8

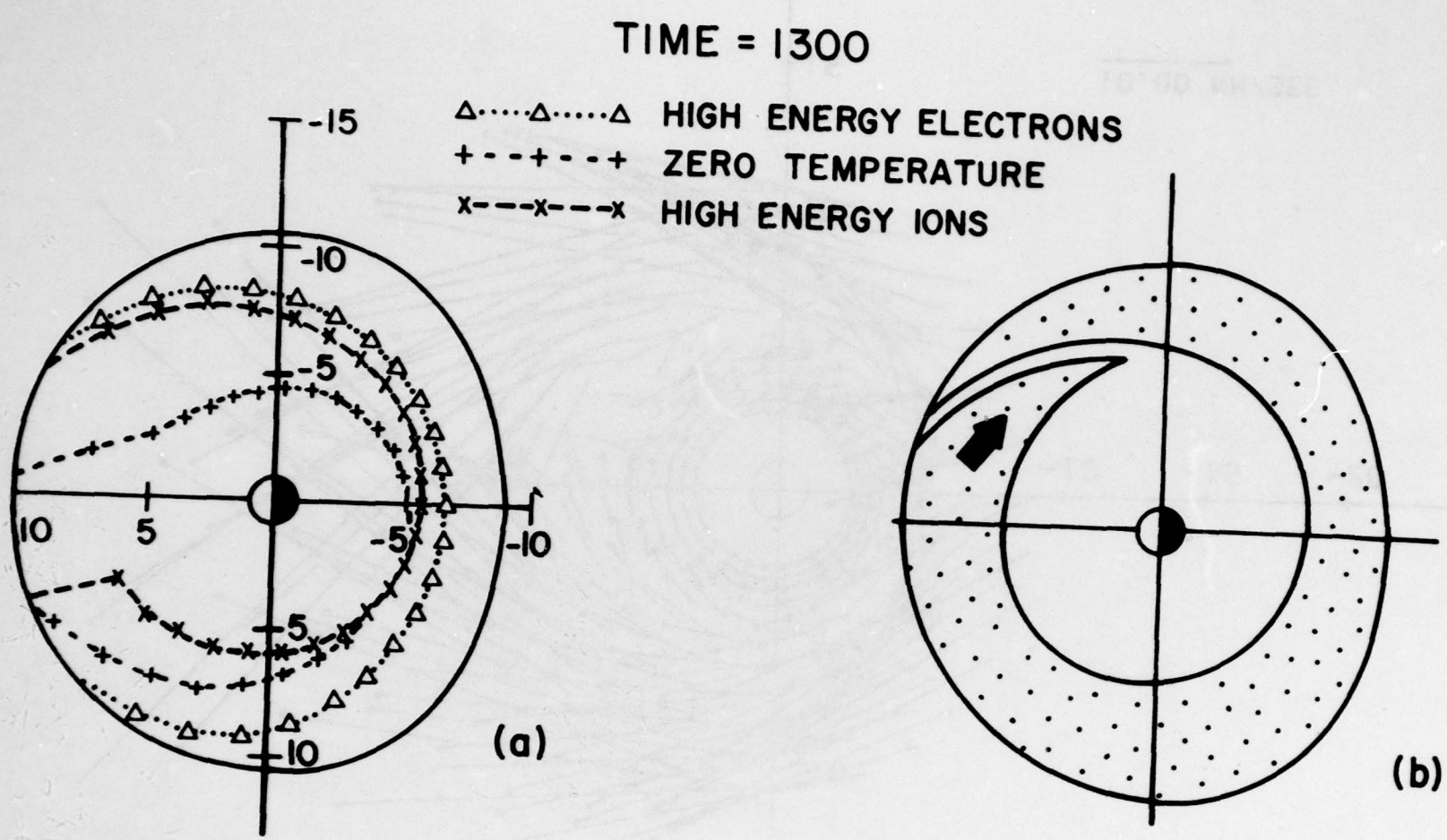
TIME = 1300
HIGH ENERGY ELECTRONS
ZERO TEMPERATURE
HIGH ENERGY IONS
-15
-10
-5
10
5
-5
-10
5
-10
(a)
(b)

Figure 9

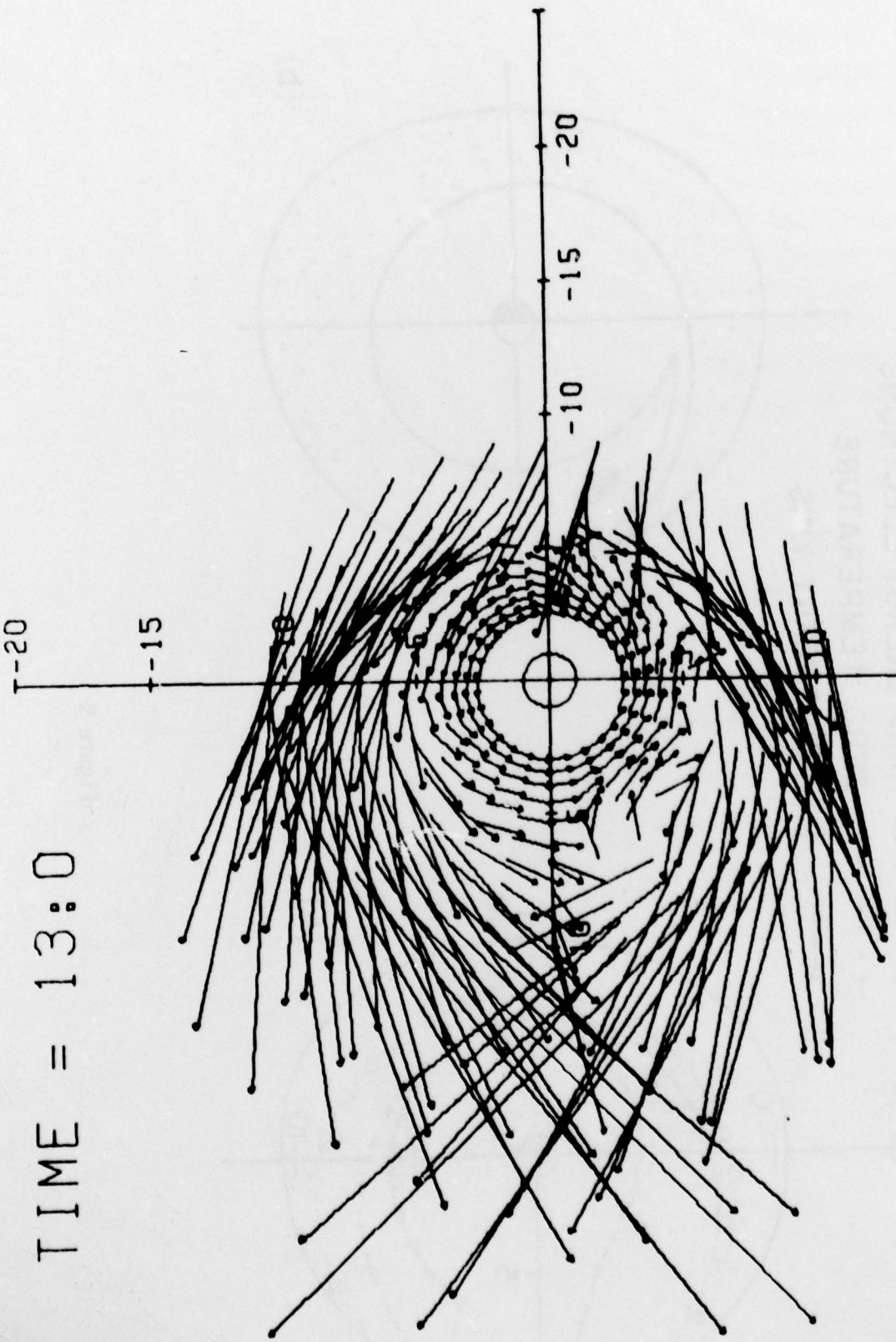

Figure 10